Phonoritonic Crystals with a Synthetic Magnetic Field for an Acoustic Diode

A. V. Poshakinskiy* and A. N. Poddubny
Ioffe Institute, Saint Petersburg 194021, Russia
(Received 30 November 2016; published 13 April 2017)

We develop a rigorous theoretical framework to describe light-sound interaction in the laser-pumped periodic multiple-quantum-well structure accounting for hybrid phonon-polariton excitations, termed phonoritons. We show that phonoritons exhibit the pumping-induced synthetic magnetic field in the artificial "coordinate-energy" space that makes transmission of left- and right- going waves different. The sound transmission nonreciprocity allows one to use such phonoritonic crystals with realistic parameters as optically controlled nanoscale acoustic diodes.

DOI: 10.1103/PhysRevLett.118.156801

Introduction.—Reciprocity is the fundamental property of waves that means the transmission coefficient invariance under the interchange of initial and final modes. Breaking of the reciprocity is required for devices, referred to as isolators or diodes, that allow wave transmission in one direction only [1,2]. Originating from the Onsager relations, the reciprocity of linear transmission persists unless the time-inversion invariance is broken or the system is driven from thermal equilibrium.

Violation of optical reciprocity can be achieved by different mechanisms, including nonlinearity [3,4], the magneto-optical effect [5–8], and mode conversion [9,10]. The proposed ways to achieve acoustic nonreciprocity are either based on nonlinearity [11–20], which requires sufficiently high signal powers, mechanical rotation [21], the temporal modulation of acoustic properties [22,23], or the introduction of a temperature gradient [24], which are difficult to realize at the nanoscale [25]. We leave aside the mode-mismatched structures [26] that, while offering asymmetric transmission, are yet formally reciprocal and therefore cannot be used for complete acoustic isolation [1].

Optomechanical resonators were shown to break the reciprocity when driven by a laser pump [39–44]. However, they require sophisticated fabrication while the problem of interfacing them with other acoustic devices remains unresolved. It was demonstrated recently that the photoelastic interaction in a multiple-quantum-well (MQW) structure is greatly enhanced by exciton resonance [45]. So far, the optomechanical effects in MQW structures have been studied only in the weak exciton-light coupling regime [46]. Here, we consider strong exciton-light coupling and add a new dimension to the phase diagram of coupled light and matter [Fig. 1(a)]. We show that this enables the realization of an optically controlled nanoscale acoustic diode and a unidirectional laser. Such MQW devices are easily integrable with existing optoelectronic platforms and might be promising for phononic computing [47].

We show that the transport of sound and light through the 1D MQW structure is equivalent to the quantum walk on a stripe of a 2D lattice in the virtual "coordinate-energy" space [41,48–53]. A finite pump laser wave vector induces a synthetic magnetic field on the 2D lattice. The field drives the transmittance nonreciprocity, akin to the quantum Hall effect.

The proposed system can be viewed as a phonoritonic crystal, a periodic lattice for phonoritons [54–57], i.e., interacting excitons, light, and sound waves, as opposed to conventional photonic, phononic, and optomechanical [58] crystals. It can controllably amplify phonons transmitted in one direction while attenuating those transmitted in the opposite direction. Sound amplification and attenuation originate from the Brillouin scattering processes and can be related to the features of the phonoriton dispersion.

Exciton-mediated light-sound interaction.—The Hamiltonian describing the interaction of excitons in a quantum well (QW) with light and longitudinal acoustic phonons reads

$$H = \omega_x b^\dagger b + \sum_q \omega_q c_q^\dagger c_q + \sum_k \Omega_k a_k^\dagger a_k + \sum_q \sqrt{\Gamma_0 c}(c_q^\dagger b + c_q b^\dagger) + \sum_k \frac{ik\Xi_k}{\sqrt{2\rho\Omega_k S}} b^\dagger b(a_k - a_k^\dagger). \quad (1)$$

The first line of the Hamiltonian (1) describes the bare excitons (bosonic annihilation operator b) with energy ω_x, free photons (c_q), and phonons (a_k) with the linear dispersion relations $\omega_q = c|q|$ and $\Omega_k = s|k|$, respectively, where c and s are the light and sound velocities in the medium, q and k are light and sound wave vectors, and $\hbar = 1$. The first term in the second line describes the exciton-light interaction in the rotating-wave approximation. The interaction strength is determined by the exciton radiative decay rate Γ_0 [59]. The last term of the Hamiltonian stands for the exciton-phonon interaction due to the deformation potential mechanism [45]. Here, Ξ_k is the deformation potential constant weighted with the

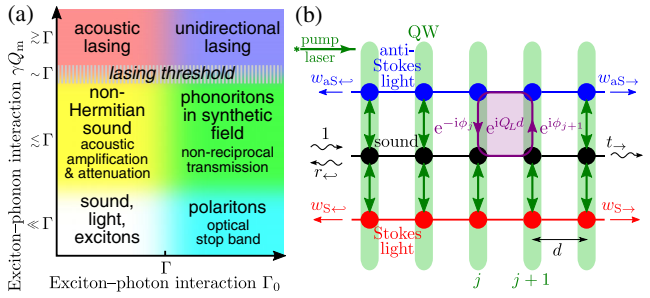

FIG. 1. (a) The regimes realized in laser-pumped MQWs, depending on the strength of the exciton-photon interaction and pumping-enhanced exciton-phonon interactions. Q_m is the mechanical quality factor. (b) Sound propagation in MQWs pumped by the laser from the left involves conversion to anti-Stokes and Stokes light and is equivalent to quantum walks on an $N \times 3$ lattice in a synthetic magnetic field.

exciton confinement wave function, ρ is the mass density, and S is the sample area [60,61].

When the MQW structure is pumped by a laser of frequency ω_L close to the exciton resonance, the coherent exciton polarization $b_{L,j} = |b_{L,j}|e^{i\phi_j}$ appears in the jth QW. We calculate these polarizations using the 2×2 transfer matrix technique for light [59]. The different regimes that can be realized depending on the strength of the exciton-light and exciton-sound interaction are summarized in Fig. 1(a). If the nonradiative broadening of the exciton Γ dominates the radiative one Γ_0, the exciton-photon interaction can be dropped out. The exciton-phonon interaction then leads to sound amplification and attenuation and gives rise to non-Hermitian acoustics, acoustic lasing at higher pump powers [46].

Here, we focus on the regime $\Gamma_0 \gtrsim \Gamma$ that is realized in state-of-the-art MQWs [45]. Consider the propagation of sound at frequency Ω in such a system. In a QW the incident sound wave can be absorbed by the exciton polarization and then radiated, giving rise to an optical wave at frequency $\omega_L + \Omega$, which we refer to as anti-Stokes light. Alternatively, the incident sound wave can stimulate the conversion of the laser-generated polarization to Stokes light with frequency $\omega_L - \Omega$. The amplitudes of these two processes are [62]

$$w_{aS(S),j} = e^{\pm i\phi_j}\sqrt{\gamma_j \Gamma_0}\,\frac{\Omega + i\Gamma_x \mp \Delta}{(\Omega + i\Gamma_x)^2 - \Delta^2 - 2\Delta i\gamma_j}, \quad (2)$$

while the amplitudes of the reciprocal processes of anti-Stokes and Stokes light conversion back to sound are $-\bar{w}_{aS(S),j}$, where the bar indicates the inversion of the sign of ϕ_j. Here, $\Delta = \omega_L - \omega_x$ is the laser detuning, $\gamma_j = |b_{L,j}|^2|\Xi_k|^2\Omega/(2\rho s^3 S)$ describes the strength of pumping-enhanced photoelastic interaction, and $\Gamma_x = \Gamma_0 + \Gamma$ is the total exciton decay rate that comprises radiative (Γ_0) and nonradiative (Γ) decay.

The sound-light conversion occurring in all of the N QWs, the initial wave transmission becomes equivalent to a quantum walk on an $N \times 3$ square lattice, see Fig. 1(b). The phase of the hopping amplitude along the artificial vertical dimension [Eq. (2)] is inherited from the phase of the laser-generated exciton polarization, $\phi_j \sim q_L dj$, where $q_L = \omega_L/c$ is the laser wave vector. Importantly, the hopping phase depends on the real dimension coordinate, i.e., the QW index j, and therefore gives rise to a synthetic magnetic field on the lattice. Indeed, consider the loop walk around the unit cell of the lattice, shown in Fig. 1(b), representing the conversion of sound to anti-Stokes light in the $(j+1)$th QW followed by back conversion in the neighboring jth QW. The amplitude of such a process is proportional to $w_{aS(S),j+1}\bar{w}_{aS(S),j}$ and has a phase $\phi_{j+1} - \phi_j \sim q_L d$. The gained phase can be viewed as the flux of some effective magnetic field. This synthetic field induces the quantum Hall effect on the lattice, yielding nonreciprocal transport.

Transfer matrix approach.—All the sound-light conversion processes that occur in a laser-pumped QW can be described by a 6×6 scattering matrix relating the output and input particle operators $(a_k, a_{-k}, c_{q_{aS}}, c_{-q_{aS}}, c^\dagger_{q_S}, c^\dagger_{-q_S})$, where $k = \Omega/s$ and $q_{aS(S)} = (\omega_L \pm \Omega)/c$ [62]. Particle creation and annihilation operators are mixed by the scattering matrix reflecting the Bogoliubov nature of the eigenstates of the optomechanical system [63]. For the multilayer system we use 6×6 transfer matrices linking the phonon and photon field operators and their spatial derivatives (a, a', c_{aS}, $c_{aS}{}'$, $c^\dagger_S$, $c_S{}'^\dagger$) on the left and right edges of a layer. Here, $f = f_{q,\text{in(out)}} + f_{-q,\text{out(in)}}$ and $f' = i[f_{q,\text{in(out)}} - f_{-q,\text{out(in)}}]$ at the left (right) of the layer; f is a, c_{aS}, or c_S. The transfer matrix of the QW reads

$$\hat{T} = \begin{pmatrix} 1 & \frac{4\gamma\Delta}{(\Omega+i\Gamma)^2-\Delta^2} & \frac{-2e^{-i\phi}\sqrt{\gamma\Gamma_0}}{\Omega+i\Gamma+\Delta} & 0 & \frac{2e^{i\phi}\sqrt{\gamma\Gamma_0}}{\Omega+i\Gamma-\Delta} & 0 \\ 0 & 1 & 0 & 0 & 0 & 0 \\ 0 & 0 & 1 & 0 & 0 & 0 \\ 0 & \frac{2e^{i\phi}\sqrt{\gamma\Gamma_0}}{\Omega+i\Gamma+\Delta} & \frac{2\Gamma_0}{\Omega+i\Gamma+\Delta} & 1 & 0 & 0 \\ 0 & 0 & 0 & 0 & 1 & 0 \\ 0 & \frac{-2e^{-i\phi}\sqrt{\gamma\Gamma_0}}{\Omega+i\Gamma-\Delta} & 0 & 0 & \frac{-2\Gamma_0}{\Omega+i\Gamma-\Delta} & 1 \end{pmatrix}. \quad (3)$$

The structure of the matrix (3) reflects the fact that the QW exciton senses the optical fields c_{aS} and $c^\dagger_S$, and the derivative of the acoustic field (i.e., the deformation) a', so they remain unchanged by the transfer matrix, while the components a, c'_{aS}, and $c'^\dagger_S$ are discontinuous at the QW position. The transfer matrix of a spacer has on the diagonal three conventional 2×2 transfer matrices, describing the free propagation of sound and light [59]. The transfer matrix for the whole MQW structure is obtained as a product of the transfer matrices of all the QWs and spacers. From that matrix the left-to-right and right-to-left sound transmission coefficients $t_\rightarrow$ and $t_\leftarrow$, as well as the

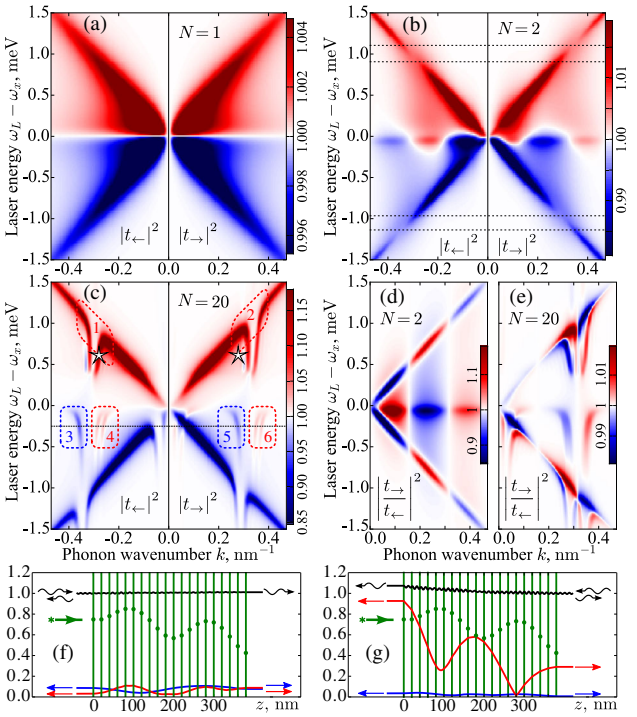

FIG. 2. (a)–(c) Dependence of the phonon transmission coefficient on the phonon wave number and pump laser frequency for different numbers of QWs N in the structure. A positive (negative) k corresponds to left-to-right (right-to-left) transmission. (d),(e) The ratio of the left-to-right and right-to-left transmittances. (f),(g) Field distributions in the processes of left-to-right and right-to-left sound transmission, respectively, for the parameters indicated by the stars in panel (c). The dots are laser-generated excitons $|b_{L,j}|$, the black line is the acoustic deformation field $|a'(z)|$, and the blue and red lines are the anti-Stokes and Stokes wave amplitudes $|c_{\mathrm{aS}}(z)|$ and $|c_{\mathrm{S}}(z)|$. The vertical lines show the QW positions. The pump density is 0.1 mW per 1 μm^2.

coefficients of sound conversion to anti-Stokes (Stokes) light, are extracted [64].

Nonreciprocal phonon transmission.—We consider now GaAs/AlAs MQW structures, studied experimentally in Refs. [45,61], with a period $d = 20$ nm and exciton parameters $\Gamma = 50$ μeV, $\Gamma_0 = 100$ μeV, $\omega_x = 1.5$ eV. Figures 2(a)–2(c) show color maps of the sound transmission coefficient for different numbers of QWs N as functions of the phonon wave vector k and the laser detuning Δ. Positive (negative) values of k represent forward (backward) acoustic transmittances $|t_{\rightarrow(\leftarrow)}(\Omega_k)|^2$. The transmission map for a single QW, Fig. 2(a), has an X-like shape: The maximal sound amplification and attenuation is realized when the phonon energy matches the laser detuning $|\Delta|$ [46], in analogy with optomechanical heating and cooling [63]. The map is symmetric with respect to the change of sign of k, meaning that the transmission through a single QW is reciprocal. This is because for a single QW there exist no walks enclosing a nonzero synthetic field flux in Fig. 1(b).

Now, we turn to the sound transmission through two QWs [Fig. 2(b)]. The corresponding transmission map is not reciprocal: an asymmetric modulation arises on top of the X-shaped feature. At small laser detuning the map is almost antireciprocal: when the right propagating phonon is amplified, the left-propagating phonon of the same frequency is attenuated and vice versa. At large laser detunings, dips appear in the X-shaped feature. The dip position is different for $|t_{\rightarrow}|^2$ and $|t_{\leftarrow}|^2$, see the dashed lines in Fig. 2(b). The nonreciprocal transmission pattern originates from the walk trajectories in Fig. 1(b) that involve conversion of sound to Stokes or anti-Stokes light in one QW followed by back conversion in the other QW. The counterclockwise (clockwise) loop paths enclose the synthetic field flux $\pm q_L d$, where $q_L = \omega_L/c$. Summation of the amplitudes corresponding to four elementary trajectories enclosing a nonzero flux gives [65]

$$\delta|t_{\rightarrow}|^2 = 2\mathrm{Re}\sum_{\sigma=\pm}\frac{-\sigma\gamma\Gamma_0}{(\sigma\Delta+\Omega+i\Gamma)^2}\cos(\sigma q_L d + kd). \qquad (4)$$

Here, the terms with $\sigma = +(-)$ correspond to the processes with the anti-Stokes (Stokes) intermediate states that dominate at positive (negative) detunings, and $q_{\mathrm{aS(S)}}d \ll 1$ was supposed. The asymmetry between the transmission for left- and right-incident phonons is driven by the pump laser that, being always incident from the left, induces the synthetic magnetic field on the lattice Fig. 1(b). In terms of the quantum walk, for any path contributing to $t_{\rightarrow}$ that encloses a synthetic field flux $q_L d$, the reciprocal path contributing to $t_{\leftarrow}$ will enclose the flux $-q_L d$. Therefore, the reciprocal transmittance $\delta|t_{\leftarrow}|^2$ is obtained from Eq. (4) by reversing the sign of q_L, which plays the role of a magnetic field. The ratio of the transmittances $|t_{\rightarrow}/t_{\leftarrow}|^2 \approx 1 + \delta|t_{\rightarrow}|^2 - \delta|t_{\leftarrow}|^2$ is shown in Fig. 2(d). In the relevant case of small $q_L d \ll 1$ it is proportional to $q_L d \sin kd$ and has extrema at $\omega_L = \omega_x$ (resonance for input light) and $\omega_L = \omega_x \pm \Omega$ (resonance for scattered light) [61].

It follows from Eq. (4) that the dips in the X-like feature appear at $|k| = \pi/d \pm q_L$. With an increase of the number of QWs N the dips enlarge, leading to the complete suppression of amplification or attenuation in a certain interval, see regions 1 and 2 in Fig. 2(c). We explain the appearance of this gap as well as the complex pattern of the transmittance in regions 3–6 by the formation of hybrid exciton-light excitations, exciton-polaritons [59]. The polariton dispersion in the infinite lossless MQW structure is shown by the black lines in Fig. 3(a). It results from an avoided crossing of the exciton dispersion, which is the horizontal line $\omega = \omega_x$, with the light dispersion, which is almost vertical, $\omega = c|q|$. The polariton dispersion is $2\pi/d$ periodic in wave vector due to the translational symmetry of the infinite MQW structure.

The pump laser generates the coherent polariton population with the wave vector $Q_L = (1/d)\arccos[\cos q_L d + (\Gamma_0/\Delta)\sin q_L d]$ [59] that follows right-propagating

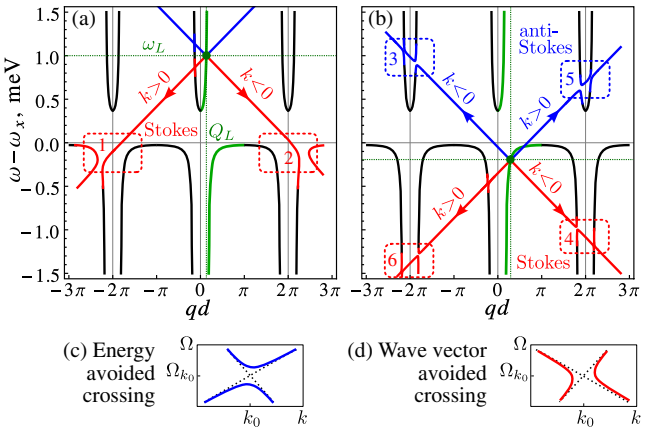

FIG. 3. (a),(b) Dispersion of polaritons (black curves), emitted and absorbed phonons (red and blue lines), and phonoritons (avoided crossings at the intersections 1–6 of the polariton and phonon dispersions). Panels (c) and (d) illustrate the two types of avoided crossings, marked by the blue and red color in panels (a) and (b), yielding the attenuation and amplification of phonons, respectively. The areas 1–6 in panels (a) and (b) explain the corresponding patterns in the phonon transmission map of Fig. 2(c). The calculation is made for laser detunings $\Delta = 1$ meV (a) and $\Delta = -0.2$ meV (b); the other parameters are the same as for Fig. 2 except for $\Gamma = 0$ and $\gamma = 20$ μeV at $\Omega = 1$ meV.

polariton dispersion, see the thick green curve. When a phonon propagates through such a pumped structure it can either be absorbed in a process of anti-Stokes polariton scattering or stimulate emission of an additional phonon in the process of Stokes scattering. Figure 3(a) shows by blue and red lines the anti-Stokes and Stokes polariton scattering processes, respectively, for the case when the laser energy is $\omega_L = \omega_x + 1$ meV. The intersections of the blue and red lines, which represent the dispersions of the absorbed and emitted phonons, respectively, with the polariton dispersion (black line) determine all possible scattering processes [61]. These processes are then manifested in the transmittance map: transmitted phonons that are resonant with anti-Stokes scattering processes are attenuated while those resonant with the Stokes process get amplified. Therefore, the pattern of the transmittance map [Fig. 2(c)] mimics the polariton dispersion.

In particular, the gaps discussed above in the transmission amplification, regions 1 and 2 in Fig. 2(c), reflect the polariton gap, which suppresses the Stokes scattering process at the corresponding frequency regions, marked in Fig. 3(a). Similarly to the case of two QWs, the position of the gap for right- and left-propagating phonons is different due to the nonzero laser-generated polariton wave vector Q_L. The transmission of sound of the same frequency can be nonresonant for left-to-right and resonant for right-to-left directions, as it occurs for the parameters indicated by stars in Fig. 2(c). Figures 2(f) and 2(g) show the field distributions in the corresponding transmission processes. The resonant case [Fig. 2(g)], in contrast to the case in Fig. 2(f), reveals intense stimulated scattering to the Stokes component and amplification of the transmitted acoustic wave. Figure 3(b) sketches the Brillouin scattering processes for the laser energy $\omega_L = \omega_x - 0.2$ meV. Both Stokes processes (regions 3 and 5) and anti-Stokes processes (regions 4 and 6) are revealed in the acoustic transmittance map as attenuation and amplification, see the corresponding regions in Fig. 2(c). The transmittance map is strongly nonreciprocal: inside the frequency band of right-propagating phonon amplification (region 6) the left-propagating phonons are attenuated (region 3), and vice versa with regions 4 and 5.

Phonoritons.—In the vicinity of the points in Fig. 3(a) where the polariton and phonon dispersions intersect, the strong photoelastic interaction modifies the eigenmodes of the system that become now phonoritons, a hybrid of a phonon and polariton [54], so far considered only in bulk crystals. The dispersion of phonoritons in the infinite MQW structure without losses can be found from the equation $\Omega^2 = \Omega_k^2 + 2\Omega_k\Sigma_k$, where the phonon self-energy correction Σ_k is readily expressed via the polariton Green's function

$$\Sigma_k = \frac{\gamma s}{d}[G(Q_L + k, \omega_L + \Omega) + G(Q_L - k, \omega_L - \Omega)],$$
$$G(K,\omega) = [\omega - \omega_x - \Gamma_0 \sin qd/(\cos Kd - \cos qd)]^{-1}. \quad (5)$$

The photoelastic interaction splits the phonoriton energy levels at the crossing points of the phonon and polariton dispersions. In the vicinity of a crossing at a phonon wave vector k_0, Eq. (5) can be linearized yielding the phonoriton dispersion $(\Omega - \Omega_k)[\Omega - \Omega_{k_0} - v_g(k - k_0)] = \delta^2$. The value of the energy level splitting 2δ is determined by the equation

$$\delta^2 = \pm\frac{\gamma v_g s}{d^2}\frac{\sin qd}{\sin Qd}\frac{\Gamma_0}{(\omega - \omega_x)^2}, \quad (6)$$

where the $+$ or $-$ sign should be chosen depending on whether the crossing of the polariton with the anti-Stokes or Stokes phonon branches is considered; $v_g = (dQ/d\omega)^{-1}$ is the polariton group velocity and all the quantities should be taken at the frequency of the crossing.

It follows from Eq. (6) that for the crossings of polaritons with anti-Stokes phonons the splitting value δ is real, while for those with Stokes phonons it is imaginary. This results in two types of avoided level crossings [66], the energy avoided crossings (red) and the wave vector avoided crossings (blue). The energy avoided crossing ($\delta^2 > 0$) is the conventional one that corresponds to the appearance of a gap for a certain frequency range, see Fig. 3(c). Propagation of the phonons inside the gap is suppressed; therefore, such an avoided crossing leads to the attenuation of the transmitted phonons. The wave vector avoided crossing ($\delta^2 < 0$) is the one when the gap appears for a certain wave vector range, see Fig. 3(d).

The gap is constrained by two exceptional points; the states with the wave vectors inside the gap have complex energies. When the amplification of these modes exceeds the losses, the system undergoes an acoustic lasing transition. Because of the strong nonreciprocity, it will emit coherent sound asymmetrically, opening the way to unidirectional acoustic lasing.

The phonoriton gaps in Fig. 3 correspond to Umklapp scattering with large phonon wave vectors $k \approx 2\pi/d$ and, therefore, a stronger deformation potential [61]. Enhancement of the phonoriton effect due to spectrum folding is the advantage of MQWs over bulk crystals. Still, realistic values of the splitting at the avoided crossings $\propto \gamma$ are much smaller than the nonradiative exciton decay Γ. Therefore, even in state-of-the-art structures the peculiarities of phonoriton dispersion are greatly broadened. Nevertheless, the sound attenuation and amplification survive in a lossy structure as an afterglow of the energy and wave vector avoided crossings, correspondingly, cf. the areas 1–6 in Figs. 2(c) and 3.

To summarize, we have introduced the concept of phonoritonic crystals featuring one-way sound transmission and unidirectional lasing. These effects are expected to be even more pronounced in new materials, e.g., stacks of transition metal dichalcogenide monolayers that possess strong exciton resonance with the radiative decay rate reaching 200 μeV [67].

The authors acknowledge fruitful discussions with A. Fainstein and S. G. Tikhodeev. This work was supported by the Russian Foundation for Basic Research Grants No. 16-32-00540 and No. 17-02-00383 and the Foundation "Dynasty." A. N. P. and A. V. P. also acknowledge support by Russian President Grants No. MK-8500.2016.2 and No. SP-2912.2016.5, respectively.

*poshakinskiy@mail.ioffe.ru

[1] A. A. Maznev, A. G. Every, and O. B. Wright, Reciprocity in reflection and transmission: What is a 'phonon diode'?, Wave Motion **50**, 776 (2013).

[2] D. Jalas, A. Petrov, M. Eich, W. Freude, S. Fan, Z. Yu, R. Baets, M. Popović, A. Melloni, J. D. Joannopoulos, M. Vanwolleghem, C. R. Doerr, and H. Renner, What is—and what is not—an optical isolator, Nat. Photonics **7**, 579 (2013).

[3] C. G. Treviño-Palacios, G. I. Stegeman, and P. Baldi, Spatial nonreciprocity in waveguide second-order processes, Opt. Lett. **21**, 1442 (1996).

[4] Y. Shi, Z. Yu, and S. Fan, Limitations of nonlinear optical isolators due to dynamic reciprocity, Nat. Photonics **9**, 388 (2015).

[5] F. D. M. Haldane and S. Raghu, Possible Realization of Directional Optical Waveguides in Photonic Crystals with Broken Time-Reversal Symmetry, Phys. Rev. Lett. **100**, 013904 (2008).

[6] T. Shintaku, Integrated optical isolator based on efficient nonreciprocal radiation mode conversion, Appl. Phys. Lett. **73**, 1946 (1998).

[7] L. Bi, J. Hu, P. Jiang, D. H. Kim, G. F. Dionne, L. C. Kimerling, and C. A. Ross, On-chip optical isolation in monolithically integrated non-reciprocal optical resonators, Nat. Photonics **5**, 758 (2011).

[8] M. Inoue, *Magnetophotonics: From Theory To Applications*, Springer Series In Materials Science (Springer, Berlin, 2013).

[9] E. Li, B. J. Eggleton, K. Fang, and S. Fan, Photonic Aharonov–Bohm effect in photon–phonon interactions, Nat. Commun. **5**, 3225 (2014).

[10] J. Kim, M. C. Kuzyk, K. Han, H. Wang, and G. Bahl, Non-reciprocal Brillouin scattering induced transparency, Nat. Phys. **11**, 275 (2015).

[11] B. Li, L. Wang, and G. Casati, Thermal Diode: Rectification of Heat Flux, Phys. Rev. Lett. **93**, 184301 (2004).

[12] B. Liang, B. Yuan, and J.-c. Cheng, Acoustic Diode: Rectification of Acoustic Energy Flux in One-Dimensional Systems, Phys. Rev. Lett. **103**, 104301 (2009).

[13] B. Liang, X. S. Guo, J. Tu, D. Zhang, and J. C. Cheng, An acoustic rectifier, Nat. Mater. **9**, 989 (2010).

[14] N. Boechler, G. Theocharis, and C. Daraio, Bifurcation-based acoustic switching and rectification, Nat. Mater. **10**, 665 (2011).

[15] B.-I. Popa and S. A. Cummer, Non-reciprocal and highly nonlinear active acoustic metamaterials, Nat. Commun. **5**, 3398 (2014).

[16] Z. Chen, C. Wong, S. Lubner, S. Yee, J. Miller, W. Jang, C. Hardin, A. Fong, J. E. Garay, and C. Dames, A photon thermal diode, Nat. Commun. **5**, 5446 (2014).

[17] C. Liu, Z. Du, Z. Sun, H. Gao, and X. Guo, Frequency-Preserved Acoustic Diode Model with High Forward-Power-Transmission Rate, Phys. Rev. Applied **3**, 064014 (2015).

[18] J. Zhang, B. Peng, Ş. K. Özdemir, Y.-x. Liu, H. Jing, X.-y. Lü, Y.-l. Liu, L. Yang, and F. Nori, Giant nonlinearity via breaking parity-time symmetry: A route to low-threshold phonon diodes, Phys. Rev. B **92**, 115407 (2015).

[19] T. Devaux, V. Tournat, O. Richoux, and V. Pagneux, Asymmetric Acoustic Propagation of Wave Packets via the Self-Demodulation Effect, Phys. Rev. Lett. **115**, 234301 (2015).

[20] Z. m. Gu, J. Hu, B. Liang, X. y. Zou, and J. c. Cheng, Broadband non-reciprocal transmission of sound with invariant frequency, Sci. Rep. **6**, 19824 (2016).

[21] R. Fleury, D. L. Sounas, C. F. Sieck, M. R. Haberman, and A. Alu, Sound isolation and giant linear nonreciprocity in a compact acoustic circulator, Science **343**, 516 (2014).

[22] M. B. Zanjani, A. R. Davoyan, A. M. Mahmoud, N. Engheta, and J. R. Lukes, One-way phonon isolation in acoustic waveguides, Appl. Phys. Lett. **104**, 081905 (2014).

[23] R. Fleury, A. B. Khanikaev, and A. Alù, Floquet topological insulators for sound, Nat. Commun. **7**, 11744 (2016).

[24] T. Biwa, H. Nakamura, and H. Hyodo, Experimental Demonstration of a Thermoacoustic Diode, Phys. Rev. Applied **5**, 064012 (2016).

[25] See Supplemental Material at http://link.aps.org/supplemental/10.1103/PhysRevLett.118.156801, which includes Refs. [26–38], for a short review of recent proposals for an acoustic diode.

[26] X.-F. Li, X. Ni, L. Feng, M.-H. Lu, C. He, and Y.-F. Chen, Tunable Unidirectional Sound Propagation through a

Sonic-Crystal-Based Acoustic Diode, Phys. Rev. Lett. **106**, 084301 (2011).
[27] R. Krishnan, S. Shirota, Y. Tanaka, and N. Nishiguchi, High-efficient acoustic wave rectifier, Solid State Commun. **144**, 194 (2007).
[28] X. Zhu, X. Zou, B. Liang, and J. Cheng, One-way mode transmission in one-dimensional phononic crystal plates, J. Appl. Phys. **108**, 124909 (2010).
[29] S. Danworaphong, T. A. Kelf, O. Matsuda, M. Tomoda, Y. Tanaka, N. Nishiguchi, O. B. Wright, Y. Nishijima, K. Ueno, S. Juodkazis, and H. Misawa, Real-time imaging of acoustic rectification, Appl. Phys. Lett. **99**, 201910 (2011).
[30] Z. He, S. Peng, Y. Ye, Z. Dai, C. Qiu, M. Ke, and Z. Liu, Asymmetric acoustic gratings, Appl. Phys. Lett. **98**, 083505 (2011).
[31] H. x. Sun, S. y. Zhang, and X. j. Shui, A tunable acoustic diode made by a metal plate with periodical structure, Appl. Phys. Lett. **100**, 103507 (2012).
[32] C. Li, M. Ke, Y. Ye, S. Xu, C. Qiu, and Z. Liu, Broadband asymmetric acoustic transmission by a plate with quasi-periodic surface ridges, Appl. Phys. Lett. **105**, 023511 (2014).
[33] I. H. Giden, D. Yilmaz, M. Turduev, H. Kurt, E. Çolak, and E. Ozbay, Theoretical and experimental investigations of asymmetric light transport in graded index photonic crystal waveguides, Appl. Phys. Lett. **104**, 031116 (2014).
[34] S. Chen, C. Hao, C. Wang, Y. Zhang, and S. Lin, One-dimensional acoustic diodes based on the anisotropy of solid media and linear acoustics, Solid State Commun. **206**, 38 (2015).
[35] S. Zhang, Y. Zhang, Y. Guo, Y. Leng, W. Feng, and W. Cao, Realization of Subwavelength Asymmetric Acoustic Transmission Based on Low-Frequency Forbidden Transmission, Phys. Rev. Applied **5**, 034006 (2016).
[36] A. J. Kent, R. N. Kini, N. M. Stanton, M. Henini, B. A. Glavin, V. A. Kochelap, and T. L. Linnik, Acoustic Phonon Emission from a Weakly Coupled Superlattice under Vertical Electron Transport: Observation of Phonon Resonance, Phys. Rev. Lett. **96**, 215504 (2006).
[37] R. P. Beardsley, A. V. Akimov, M. Henini, and A. J. Kent, Coherent Terahertz Sound Amplification and Spectral Line Narrowing in a Stark Ladder Superlattice, Phys. Rev. Lett. **104**, 085501 (2010).
[38] W. Maryam, A. V. Akimov, R. P. Campion, and A. J. Kent, Dynamics of a vertical cavity quantum cascade phonon laser structure, Nat. Commun. **4**, 2184 (2013).
[39] M. Hafezi and P. Rabl, Optomechanically induced non-reciprocity in microring resonators, Opt. Express **20**, 7672 (2012).
[40] S. J. M. Habraken, K. Stannigel, M. D. Lukin, P. Zoller, and P. Rabl, Continuous mode cooling and phonon routers for phononic quantum networks, New J. Phys. **14**, 115004 (2012).
[41] M. Schmidt, S. Kessler, V. Peano, O. Painter, and F. Marquardt, Optomechanical creation of magnetic fields for photons on a lattice, Optica **2**, 635 (2015).
[42] V. Peano, C. Brendel, M. Schmidt, and F. Marquardt, Topological Phases of Sound and Light, Phys. Rev. X **5**, 031011 (2015).
[43] F. Ruesink, M.-A. Miri, A. Alù, and E. Verhagen, Non-reciprocity and magnetic-free isolation based on optomechanical interactions, Nat. Commun. **7**, 13662 (2016).
[44] Z. Shen, Y.-L. Zhang, Y. Chen, C.-L. Zou, Y.-F. Xiao, X.-B. Zou, F.-W. Sun, G.-C. Guo, and C.-H. Dong, Experimental realization of optomechanically induced non-reciprocity, Nat. Photonics **10**, 657 (2016).
[45] B. Jusserand, A. N. Poddubny, A. V. Poshakinskiy, A. Fainstein, and A. Lemaitre, Polariton Resonances for Ultrastrong Coupling Cavity Optomechanics in GaAs/AlAs Multiple Quantum Wells, Phys. Rev. Lett. **115**, 267402 (2015).
[46] A. V. Poshakinskiy, A. N. Poddubny, and A. Fainstein, Multiple Quantum Wells for $\mathcal{PT}$-Symmetric Phononic Crystals, Phys. Rev. Lett. **117**, 224302 (2016).
[47] S. R. Sklan, Splash, pop, sizzle: Information processing with phononic computing, AIP Adv. **5**, 053302 (2015).
[48] O. Boada, A. Celi, J. I. Latorre, and M. Lewenstein, Quantum Simulation of an Extra Dimension, Phys. Rev. Lett. **108**, 133001 (2012).
[49] A. Celi, P. Massignan, J. Ruseckas, N. Goldman, I. B. Spielman, G. Juzeliunas, and M. Lewenstein, Synthetic Gauge Fields in Synthetic Dimensions, Phys. Rev. Lett. **112**, 043001 (2014).
[50] X.-W. Luo, X. Zhou, C.-F. Li, J.-S. Xu, G.-C. Guo, and Z.-W. Zhou, Quantum simulation of 2D topological physics in a 1D array of optical cavities, Nat. Commun. **6**, 7704 (2015).
[51] L. Yuan, Y. Shi, and S. Fan, Photonic gauge potential in a system with a synthetic frequency dimension, Opt. Lett. **41**, 741 (2016).
[52] T. Ozawa, H. M. Price, N. Goldman, O. Zilberberg, and I. Carusotto, Synthetic dimensions in integrated photonics: From optical isolation to four-dimensional quantum hall physics, Phys. Rev. A **93**, 043827 (2016).
[53] T. Ozawa and I. Carusotto, Synthetic dimensions with magnetic fields and local interactions in photonic lattices, Phys. Rev. Lett. **118**, 013601 (2017).
[54] A. L. Ivanov and L. V. Keldysh, Restructuring of polariton and phonon spectra of a semiconductor in the presence of a strong electromagnetic wave, Zh. Eksp. Teor. Fiz. **84**, 404 (1983) [Sov. Phys. JETP **57**, 234 (1983)].
[55] L. V. Keldysh and S. G. Tikhodeev, High-intensity polariton wave near the stimulated scattering threshold, Zh. Eksp. Teor. Fiz. **90**, 1852 (1986) [Sov. Phys. JETP **63**, 1086 (1986)].
[56] G. S. Vygovskiĭ, G. P. Golubev, E. A. Zhukov, A. A. Fomichev, and M. A. Yakshin, Phonoriton modification of the polariton dispersion curve in CdS, Pis'ma Zh. Eksp. Teor. Fiz. **42**, 134 (1985) [JETP Lett. **42**, 164 (1985)].
[57] L. Hanke, D. Fröhlich, A. L. Ivanov, P. B. Littlewood, and H. Stolz, LA phonoritons in Cu_2O, Phys. Rev. Lett. **83**, 4365 (1999).
[58] M. Eichenfield, J. Chan, R. M. Camacho, K. J. Vahala, and O. Painter, Optomechanical crystals, Nature (London) **462**, 78 (2009).
[59] E. L. Ivchenko, *Optical Spectroscopy of Semiconductor Nanostructures* (Alpha Science International, Harrow, UK, 2005).
[60] B. Jusserand, Selective resonant interaction between confined excitons and folded acoustic phonons in GaAs/AlAs multi-quantum wells, Appl. Phys. Lett. **103**, 093112 (2013).

[61] A. N. Poddubny, A. V. Poshakinskiy, B. Jusserand, and A. Lemaître, Resonant Brillouin scattering of excitonic polaritons in multiple-quantum-well structures, Phys. Rev. B **89**, 235313 (2014).

[62] See Supplemental Material at http://link.aps.org/supplemental/10.1103/PhysRevLett.118.156801 for the derivation of the sound and light transmission, reflection, and conversion amplitudes by means of the Keldysh diagram technique.

[63] M. Aspelmeyer, T. J. Kippenberg, and F. Marquardt, Cavity optomechanics, Rev. Mod. Phys. **86**, 1391 (2014).

[64] See Supplemental Material at http://link.aps.org/supplemental/10.1103/PhysRevLett.118.156801 for the expression of the transmission and conversion coefficients through transfer matrix elements.

[65] See Supplemental Material at http://link.aps.org/supplemental/10.1103/PhysRevLett.118.156801 for the derivation of the amplitudes.

[66] B. S. Wang and J. L. Birman, Theory of phonoritons and experiments to determine phonoriton dispersion and spectrum, Phys. Rev. B **42**, 9609 (1990).

[67] C. Robert, D. Lagarde, F. Cadiz, G. Wang, B. Lassagne, T. Amand, A. Balocchi, P. Renucci, S. Tongay, B. Urbaszek, and X. Marie, Exciton radiative lifetime in transition metal dichalcogenide monolayers, Phys. Rev. B **93**, 205423 (2016).